

Can we Adopt Self-supervised Pretraining for Chest X-Rays?

Arsh Verma

Makarand Tapaswi

Wadhvani Institute for Artificial Intelligence (Wadhvani AI), India

ARSH@WADHWANAI.ORG and

MAKARAND@WADHWANAI.ORG

Abstract

Chest radiograph (or Chest X-Ray, CXR) is a popular medical imaging modality that is used by radiologists across the world to diagnose heart or lung conditions. Over the last decade, Convolutional Neural Networks (CNN), have seen success in identifying pathologies in CXR images. Typically, these CNNs are pretrained on the standard ImageNet classification task, but this assumes availability of large-scale annotated datasets. In this work, we analyze the utility of pretraining on *unlabeled* ImageNet or Chest X-Ray (CXR) datasets using various algorithms and in multiple settings. Some findings of our work include: (i) supervised training with labeled ImageNet learns strong representations that are hard to beat; (ii) self-supervised pretraining on ImageNet ($\sim 1\text{M}$ images) shows performance similar to self-supervised pretraining on a CXR dataset ($\sim 100\text{K}$ images); and (iii) the CNN trained on supervised ImageNet can be trained further with self-supervised CXR images leading to improvements, especially when the downstream dataset is on the order of a few thousand images.

Keywords: Chest X-Ray, Self-Supervised Pretraining

1. Introduction

Modern medicine uses advanced medical imaging techniques to assist physicians in disease diagnosis. In particular, chest radiography (or Chest X-Rays, CXR) is a pop-

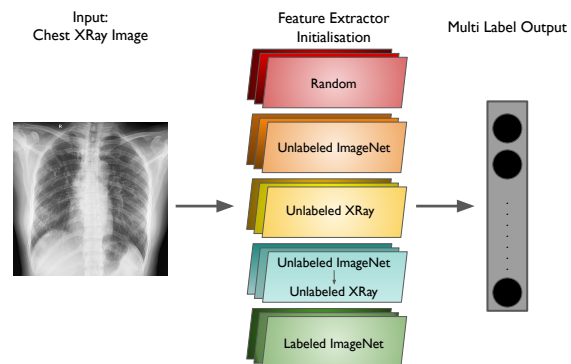


Figure 1: Overview of various training or initialization strategies adopted in our work for multi-label classification in Chest X-rays.

ular modality to identify pathologies in the lungs or heart owing to its low cost and decent availability (Ngoya et al., 2016; Smith-Bindman et al., 2012). Unfortunately, the number of X-Rays performed every year are rapidly rising, while the number of skilled radiologists required to analyze them is not keeping pace (Henderson, 2022).

This has spurred interest among Machine Learning researchers to develop models for automated detection of pathologies (*e.g. consolidation*) in Chest X-Rays (Rajpurkar et al., 2017; Lakhani and Sundaram, 2017; Tang et al., 2020). However, today’s deep models are data hungry and while there is an abundance of X-Ray images, labeling them is a severe bottleneck. Obtaining gold standard labels requires hiring several radiologists, who may still disagree with each other (Albaum et al., 1996; Johnson and Kline, 2010), leading to potentially er-

roneous labels (Brady, 2017). Such large datasets may also be annotated automatically with NLP parsers based on radiological reports (Johnson et al., 2019; Irvin et al., 2019), have varying prevalence for labels, and may also have differing imaging properties. Finally, relying on a set of annotations limits predictions to a closed set of labels, which are often different across datasets (*cf.* Appendix A).

A common practice to reduce the requirement of large labeled in-domain datasets is *transfer learning* where models pretrained on one task are used for initializing models on the target task (Raghu et al., 2019; Matsoukas et al., 2022; Sellergren et al., 2022). With over a million images spanning thousand classes, ImageNet (Deng et al., 2009) has emerged as the *de facto* pretraining dataset for vision tasks and is surprisingly effective even for medical imaging problems.

As an alternative to labeling large-scale image datasets, self-supervised learning (SSL) has shown promise in learning features on a proxy task such as distinguishing a paired augmentation of the same image against other images (Chen et al., 2020).

Findings. As illustrated in Fig. 1, we wish to investigate the effect of using SSL pre-training (PT) on in-domain CXR *vs.* out-of-domain datasets. We denote SSL PT to mean pretraining with a self-supervised objective. We conduct such experiments on two CXR datasets (see Table 1) and identify three key takeaways: (i) SSL PT on the ImageNet or NIH dataset outperforms training from scratch by a large gap; (ii) SSL PT on ImageNet ($\sim 1\text{M}$ images) achieves comparable performance to SSL PT on the NIH dataset ($\sim 100\text{K}$ images); and (iii) SSL PT on ImageNet followed by SSL PT on the in-domain NIH improves downstream performance.

We also compare SSL against supervised learning, and find that SSL methods lag be-

Table 1: Details of Chest X-Ray datasets.

| Dataset | # Samples | # Labels |
|-------------------------------|-----------|----------|
| NIH-CXR (Summers, 2019) | 112,120 | 11 |
| CheXpert (Irvin et al., 2019) | 224,316 | 12 |

hind (sometimes only by a small margin) supervised ImageNet PT. However, SSL PT on in-domain CXR data provides small but consistent improvements to the supervised ImageNet representations.

Finally, we present two additional analyses: (i) the number of labels used for evaluation (5 *vs.* all) has a small influence on the gap between SSL PT *vs.* supervised ImageNet performance; and

(ii) zero-shot evaluation of models finetuned on one CXR dataset to another shows that SSL PT learns robust models.

Related SSL works in CXR. Recently, there have been significant efforts to explore related directions of supervised contrastive learning (Khosla et al., 2020), applying augmentations based on medical records, *e.g.* in the form of multiple views (Vu et al., 2021; Azizi et al., 2021), learning from images and their reports (Zhang et al., 2020), applying SSL methods to adapt pretrained ImageNet models to the CXR domain (Sowrirajan et al., 2021; Gazda et al., 2021; Reed et al., 2022), and even a review of SSL applications in the medical domain (Krishnan et al., 2022). Our work is similar to the multi-stage training strategy of Reed et al. (2022), but we use *unlabeled generalist* pretraining on an out-of-domain dataset and *unlabeled specialist* pretraining on an in-domain dataset. Azizi et al. (2021) also perform SSL PT on ImageNet followed by SSL PT on CheXpert. Interestingly, while they obtain small improvements (with 5 labels), we see that supervised learning surpasses SSL PT when using all labels, while the two come close when using 5 labels.

2. Experimental Setup

We present the datasets, methods, and implementation details used in this study.

Datasets. We formulate Chest X-Ray pathology detection as a multi-label classification problem, where the list of labels is specific to each dataset. We perform experiments primarily on NIH-CXR (Wang et al., 2017; Summers, 2019) and CheXpert (Irvin et al., 2019), where the list of labels in each dataset (post combination based on inputs from a radiologist) is presented in Table 3 (Appendix A). We split the data into 80:10:10 between train, validation and test while ensuring subjects are disjoint.

SSL Methods. We demonstrate results on 5 different SSL algorithms. We apply a limited set of augmentations to CXR images: horizontal flipping and rotation, as the data is already in grayscale, and addition of noise and blur may negatively affect performance (Sowrirajan et al., 2021). We will see that even with these few and simple augmentations, pretraining on in-domain data shows comparable performance.

(i) **SimCLR** (Chen et al., 2020) is among the first SSL contrastive learning approaches. It aims to maximize similarity between representations of two augmentations of the same image in the latent space via a contrastive loss function, while all other images in the minibatch are treated as negative pairs. (ii) **MoCo** (He et al., 2020) also uses two augmented views of an image but pairs them with two encoders, where the parameter updates for the momentum encoder are performed through a linear interpolation between the two encoders.

The previous methods apply contrastive learning at an instance level and use negative samples in their formulation. Different from them, (iii) **SwAV** (Caron et al., 2020) creates multiple clusters to partition the dataset, and attempts to map all aug-

mented views of the same image to the same cluster, called prototype. (iv) **BYOL** (Grill et al., 2020) uses two networks - online and target - which have the same architecture. Here, the target network is used to teach the online network to correctly predict an augmented view of the same image. Finally, (v) **SimSiam** (Chen and He, 2021) uses two parallel encoders to generate representations of augmented views of the same image. However, gradient propagation is prevented in one encoder through the use of the Stop-Gradient operator.

Fine-tuning data subsets. Our PT models are fine-tuned on different proportions of the NIH or CheXpert training sets. We use subsets 1%, 10%, or 100% of the training set to analyze the impact of fine-tuning on smaller subsets of the data. For SSL PT, we use the entire 100% NIH training set.

Training details. Images are resized to 224×224 resolution for training. We use a ResNet50 backbone followed by a linear layer for all our multi-label classification models, and adopt the Binary Cross-Entropy loss. We perform ImageNet pretraining using (MMSelfSup, 2021) and follow the same settings for NIH. Following this, we perform supervised fine-tuning on different CXR datasets - NIH and CheXpert (CheX). The models are fine-tuned for 30 epochs, with a learning rate of $1e-4$, decayed by half every 5 epochs, and the Adam optimizer. Hyperparameters are tuned on the validation set.

Zero-shot experiments. We evaluate models fine-tuned on one dataset (*e.g.* NIH) on another dataset (*e.g.* CheXpert) to understand the zero-shot transfer capability. As necessary, we restrict to the set of commonly used 5 labels (Irvin et al., 2019).

Metrics. We report the mean AUROC to compare results for all experiments as in past literature (*e.g.* (Rajpurkar et al., 2018)).

Table 2: Comparison between models pretrained with different paradigms on NIH and CheXpert (CheX). During PT, NIH corresponds to 100% of the train set. Supervised PT uses a standard classification setup for ImageNet (ImNet). The number in green is the best result with supervised ImageNet PT, and the number in blue is the best SSL PT strategy.

| Algorithm | Pre-training Dataset | | Finetuning Dataset | | | | | |
|-----------|----------------------|--------------|--------------------|---------|----------|---------|----------|-----------|
| | Supervised | Unsupervised | NIH 1% | NIH 10% | NIH 100% | CheX 1% | CheX 10% | CheX 100% |
| 1 | - | - | 0.5566 | 0.6794 | 0.7886 | 0.5582 | 0.6480 | 0.7534 |
| 2 | ImNet | - | 0.6851 | 0.8026 | 0.8538 | 0.6916 | 0.7589 | 0.8066 |
| 3 | - | ImNet | 0.5818 | 0.6917 | 0.8297 | 0.5738 | 0.7123 | 0.7902 |
| 4 | SimCLR | NIH | 0.5916 | 0.7481 | 0.8291 | 0.6497 | 0.7314 | 0.7833 |
| 5 | | ImNet → NIH | 0.6109 | 0.7585 | 0.8435 | 0.6117 | 0.7471 | 0.7990 |
| 6 | | NIH | 0.7151 | 0.8097 | 0.8559 | 0.7170 | 0.7665 | 0.8089 |
| 7 | - | ImNet | 0.5711 | 0.7031 | 0.8293 | 0.5643 | 0.7158 | 0.7933 |
| 8 | SwAV | NIH | 0.5880 | 0.7207 | 0.8384 | 0.6004 | 0.7328 | 0.7911 |
| 9 | | ImNet → NIH | 0.6304 | 0.7591 | 0.8496 | 0.6142 | 0.7468 | 0.8000 |
| 10 | | NIH | 0.6347 | 0.8035 | 0.8540 | 0.6523 | 0.7569 | 0.8072 |
| 11 | - | ImNet | 0.5861 | 0.7219 | 0.8362 | 0.5744 | 0.7289 | 0.7938 |
| 12 | BYOL | NIH | 0.6017 | 0.7154 | 0.8305 | 0.5786 | 0.7272 | 0.7889 |
| 13 | | ImNet → NIH | 0.5918 | 0.7651 | 0.8445 | 0.6045 | 0.7449 | 0.7996 |
| 14 | | NIH | 0.6783 | 0.7779 | 0.8496 | 0.6798 | 0.7614 | 0.8052 |
| 15 | - | ImNet | 0.5711 | 0.7087 | 0.8359 | 0.6033 | 0.7324 | 0.7977 |
| 16 | MoCo v2 | NIH | 0.5841 | 0.719 | 0.8041 | 0.6373 | 0.7085 | 0.7607 |
| 17 | | ImNet → NIH | 0.6258 | 0.7343 | 0.8379 | 0.6382 | 0.7417 | 0.7992 |
| 18 | | NIH | 0.7061 | 0.8093 | 0.8569 | 0.7142 | 0.7666 | 0.8077 |
| 19 | - | ImNet | 0.5192 | 0.5630 | 0.7434 | 0.5503 | 0.6507 | 0.7659 |
| 20 | SimSiam | NIH | 0.5143 | 0.5833 | 0.7852 | 0.5241 | 0.639 | 0.7586 |
| 21 | | ImNet → NIH | 0.5358 | 0.7039 | 0.8028 | 0.6244 | 0.7091 | 0.7668 |
| 22 | | NIH | 0.5835 | 0.7796 | 0.8478 | 0.6714 | 0.7542 | 0.8036 |

3. Results and Discussion

Table 2 reports results for various combinations of pretraining and fine-tuning strategies on both NIH and CheXpert datasets.

Supervised PT on ImageNet, an out-of-domain dataset, strongly benefits model performance. The difference in AUROC when training from scratch (row 1) *vs.* using ImageNet initialization (row 2) is 13-14% (absolute AUROC points) for the small data subsets of NIH 1% and CheX 1%. While this reduces progressively, there is a notable

5-7% gap even for the entire training set (NIH 100% or CheX 100%).

Does SSL ImageNet PT help? Yes. Rows 3, 7, 11, and 15 show a consistent 3-5% performance improvement over row 1 (training from scratch). Interestingly SimSiam (row 19) is the only SSL method that hurts performance – perhaps the domain gap is too large for the stop-gradient based training with parameter updates.

Comparing NIH *vs.* ImageNet PT. Pairs of rows 3-4, 7-8, 11-12, and 15-16 allow us to compare the impact of in-domain (NIH) *vs.* out-of-domain (ImageNet) pretraining.

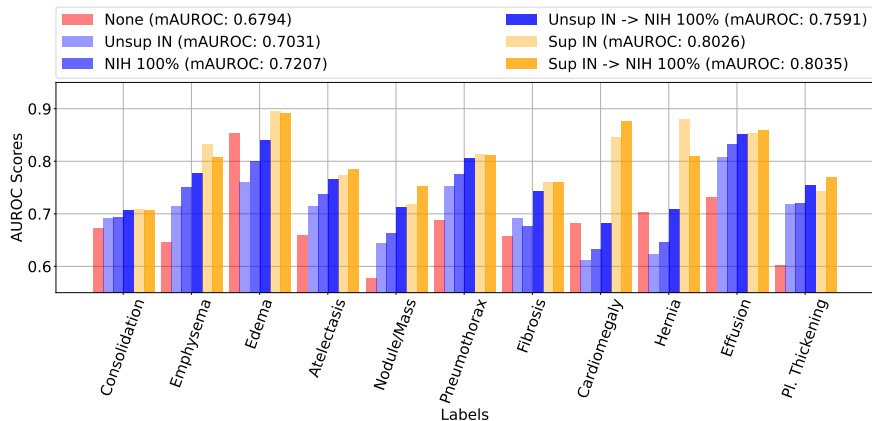


Figure 2: Per-label AUROC. SSL PT algorithm: SwAV, Finetuning: NIH 10% dataset.

Note that ImageNet has about 1M images while NIH has less than 100K images. We see largely comparable performance or small improvements of 0.5-1% when fine-tuning on NIH, indicating the efficiency of a smaller in-domain PT dataset. Importantly, in-domain PT shows a substantial improvement of 3-8% over a model trained from scratch (row 1). For CheXpert, while SimCLR, SwAV, and BYOL show 3-7% improvements for CheX 1%, when using the full CheX 100% for training, ImageNet PT models are comparable or better.

Does chaining SSL PT strategies improve performance? We compare ImNet \rightarrow NIH (rows 5, 9, 13, 17) against their individual ImageNet only or NIH only variants. Barring a few exceptions, we see consistent improvements ranging from 0.5-5% by chaining the PT strategies for all methods. This verifies that the hierarchical pretraining strategy suggested by Reed et al. (2022) is also applicable when both PT datasets are used in the self-supervised mode. With this method, and when using 100% of the fine-tuning datasets, we observe that SSL PT models are less than 1% away from supervised ImageNet PT (row 2).

Is it possible to chain SSL in-domain PT with supervised ImageNet PT? Yes, in fact, row 6 (SimCLR) seems to achieve the

best performance across 5 of the 6 settings, with row 18 (MoCo v2) being a close second in 2 settings. We see larger improvements of 3% and 2.6% on the NIH 1% and CheX 1% subsets, however, these shrink when using the entire training set to 0.2-0.3%.

Which SSL method is the best? As expected, there is not one method that performs best in all scenarios. However, SwAV seems to perform well in the SSL only settings, while SimCLR chains well with supervised ImageNet achieving good performance across all settings. SimSiam underperforms on all fine-tuning results.

Cross-dataset evaluation. As seen in the comparison between in-domain and out-of-domain PT, we note that the PT dataset is always NIH even when we fine-tune on CheXpert. It is encouraging to see that PT on a different CXR image dataset still helps improve performance on CheXpert.

Labelwise performance. Fig. 2 shows the AUROC for individual labels when fine-tuned on the NIH 10% dataset. It is encouraging to observe that chaining unsupervised ImageNet and NIH PT (dark blue bar) outperforms SSL PT on individual datasets across each label. However, the same cannot be said for the supervised ImageNet settings (yellow bars). Looking at the individual labels, we see a large variation in perfor-

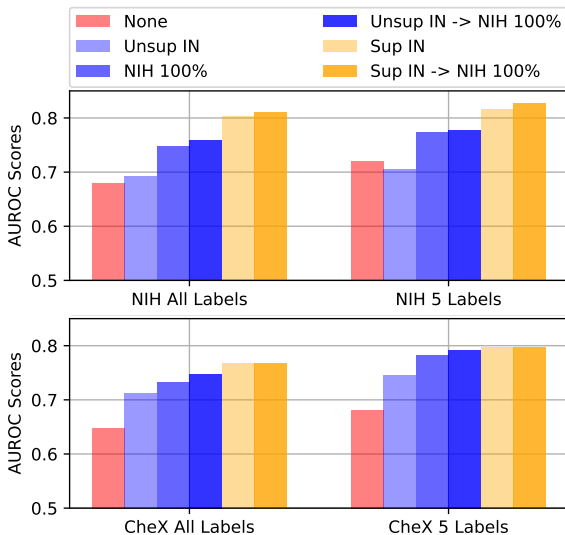


Figure 3: Comparing fine-tuning on 5 *vs.* all labels using the SimCLR algorithm. Top: NIH, Bottom: CheXpert.

mance - interestingly, this is not only driven by the number of instances that are available for each pathology.

Comparison of 5 *vs.* all labels. Fig. 3 shows the results when evaluating on 5 or all labels. As expected, all results improve when looking at a subset of 5 labels that appear often or are more important (Irvin et al., 2019). Interestingly, the gap between the models trained using the SSL PT strategy (blue bars) and supervised ImageNet models (light yellow bar) reduces as we transition from All to 5 labels for CheXpert. We are not sure why this may happen.

Zero-shot evaluation. Finally, we present an experiment where fine-tuned models are evaluated across datasets. In Fig. 4, we show results for models fine-tuned on NIH data on MIMIC-CXR (Johnson et al., 2019) and CheXpert (using 5 labels as there are different labels in these datasets), and a model fine-tuned on CheXpert evaluated on MIMIC with all labels (as they have the same label set). We observe that models that have been trained with in-domain SSL PT methods (dark blue and blue bars) outperform

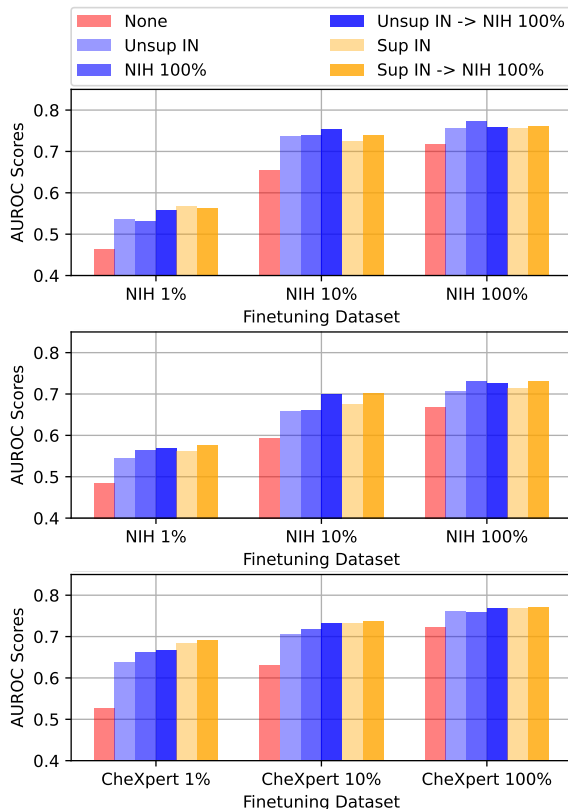


Figure 4: Zero-shot evaluation. Models are PT using the SwAV algorithm. Top: NIH \rightarrow MIMIC (5 labels). Middle: NIH \rightarrow CheXpert (5 labels). Bottom: CheXpert \rightarrow MIMIC (all labels).

even supervised ImageNet PT. This indicates that such models may be more robust to deploy in real-world scenarios as they are less affected by domain shifts in the dataset.

Conclusion. We evaluated various supervised and self-supervised pretraining strategies for CXR datasets and showed the effects of in-domain and out-of-domain pretraining.

Acknowledgements. This work is made possible by the generous support of the American people through the United States Agency for International Development (USAID). The contents are the responsibility of Wadhvani AI and do not necessarily reflect the views of USAID or the United States Government.

References

- Michael N Albaum, Lisa C Hill, Miles Murphy, Yi-Hwei Li, Carl R Fuhrman, Cynthia A Britton, Wishwa N Kapoor, and Michael J Fine. Interobserver Reliability of the Chest Radiograph in Community-Acquired Pneumonia. *Chest*, 110(2):343–350, 1996.
- Shekoofeh Azizi, Basil Mustafa, Fiona Ryan, Zachary Beaver, Jan Freyberg, Jonathan Deaton, Aaron Loh, Alan Karthikesalingam, Simon Kornblith, Ting Chen, et al. Big Self-Supervised Models Advance Medical Image Classification. In *IEEE/CVF International Conference on Computer Vision (ICCV)*, pages 3478–3488, 2021.
- Adrian P Brady. Error and Discrepancy in Radiology: Inevitable or Avoidable? *Insights into Imaging*, 8(1):171–182, 2017.
- Mathilde Caron, Ishan Misra, Julien Mairal, Priya Goyal, Piotr Bojanowski, and Armand Joulin. Unsupervised Learning of Visual Features by Contrasting Cluster Assignments. In *Advances in Neural Information Processing Systems (NeurIPS)*, pages 9912–9924, 2020.
- Ting Chen, Simon Kornblith, Mohammad Norouzi, and Geoffrey Hinton. A Simple Framework for Contrastive Learning of Visual Representations. In *International Conference on Machine Learning (ICML)*, pages 1597–1607, 2020.
- Xinlei Chen and Kaiming He. Exploring Simple Siamese Representation Learning. In *IEEE/CVF Conference on Computer Vision and Pattern Recognition (CVPR)*, pages 15750–15758, 2021.
- Jia Deng, Wei Dong, Richard Socher, Li-Jia Li, Kai Li, and Li Fei-Fei. ImageNet: A Large-scale Hierarchical Image database. In *IEEE/CVF Conference on Computer Vision and Pattern Recognition*, pages 248–255, 2009.
- Matej Gazda, Ján Plavka, Jakub Gazda, and Peter Drotar. Self-Supervised Deep Convolutional Neural Network for Chest X-Ray Classification. *IEEE Access*, 9: 151972–151982, 2021.
- Jean-Bastien Grill, Florian Strub, Florent Altché, Corentin Tallec, Pierre Richemond, Elena Buchatskaya, Carl Doersch, Bernardo Avila Pires, Zhaohan Guo, Mohammad Gheshlaghi Azar, et al. Bootstrap Your Own Latent-A New Approach to Self-Supervised Learning. In *Advances in Neural Information Processing Systems (NeurIPS)*, pages 21271–21284, 2020.
- Kaiming He, Haoqi Fan, Yuxin Wu, Saining Xie, and Ross Girshick. Momentum Contrast for Unsupervised Visual Representation Learning. In *IEEE/CVF Conference on Computer Vision and Pattern Recognition (CVPR)*, pages 9729–9738, 2020.
- Mary Henderson. Radiology Facing a Global Shortage. <https://www.rsna.org/news/2022/may/Global-Radiologist-Shortage>, Last accessed: 23/11/2022], 2022.
- Jeremy Irvin, Pranav Rajpurkar, Michael Ko, Yifan Yu, Silvana Ciurea-Ilcus, Chris Chute, Henrik Marklund, Behzad Haggoo, Robyn Ball, Katie Shpanskaya, et al. Chexpert: A Large Chest Radiograph Dataset with Uncertainty Labels and Expert Comparison. In *AAAI Conference on Artificial Intelligence (AAAI)*, pages 590–597, 2019.
- Alistair EW Johnson, Tom J Pollard, Seth J Berkowitz, Nathaniel R Greenbaum, Matthew P Lungren, Chih-ying

- Deng, Roger G Mark, and Steven Horng. MIMIC-CXR, A De-identified publicly available database of Chest Radiographs with free-text reports. *Scientific Data*, 6 (1), 2019.
- Jeremiah Johnson and Jeffrey A Kline. Intraobserver and Interobserver Agreement of the Interpretation of Pediatric Chest Radiographs. *Emergency Radiology*, 17(4): 285–290, 2010.
- Prannay Khosla, Piotr Teterwak, Chen Wang, Aaron Sarna, Yonglong Tian, Phillip Isola, Aaron Maschinot, Ce Liu, and Dilip Krishnan. Supervised Contrastive Learning. In *Advances in Neural Information Processing Systems (NeurIPS)*, pages 18661–18673, 2020.
- Rayan Krishnan, Pranav Rajpurkar, and Eric J Topol. Self-Supervised Learning in Medicine and Healthcare. *Nature Biomedical Engineering*, pages 1–7, 2022.
- Paras Lakhani and Baskaran Sundaram. Deep Learning at Chest Radiography: Automated Classification of Pulmonary Tuberculosis by using Convolutional Neural Networks. *Radiology*, 284(2):574–582, 2017.
- Christos Matsoukas, Johan Fredin Haslum, Moein Sorkhei, Magnus Söderberg, and Kevin Smith. What Makes Transfer Learning Work For Medical Images: Feature Reuse & Other Factors. In *IEEE/CVF Conference on Computer Vision and Pattern Recognition*, pages 9225–9234, 2022.
- MMSelfSup. MMSelfSup: Openmmlab self-supervised learning toolbox and benchmark. <https://github.com/open-mmlab/mmselfsup>, 2021.
- Patrick Sitati Ngoya, Wilbroad Edward Muhogora, and Richard Denys Pitcher. Defining the Diagnostic Divide: An Analysis of Registered Radiological Equipment Resources in a Low-income African country. *The Pan African Medical Journal*, 25, 2016.
- Maithra Raghu, Chiyuan Zhang, Jon Kleinberg, and Samy Bengio. Transfusion: Understanding Transfer Learning for Medical Imaging. In *Advances in Neural Information Processing Systems (NeurIPS)*, 2019.
- Pranav Rajpurkar, Jeremy Irvin, Kaylie Zhu, Brandon Yang, Hershel Mehta, Tony Duan, Daisy Ding, Aarti Bagul, Curtis Langlotz, Katie Shpanskaya, et al. Chexnet: Radiologist-level Pneumonia Detection on Chest X-Rays with Deep Learning. *arXiv preprint arXiv:1711.05225*, 2017.
- Pranav Rajpurkar, Jeremy Irvin, Robyn L Ball, Kaylie Zhu, Brandon Yang, Hershel Mehta, Tony Duan, Daisy Ding, Aarti Bagul, Curtis P Langlotz, et al. Deep Learning for Chest Radiograph Diagnosis: A Retrospective Comparison of the CheXNeXt Algorithm to Practicing Radiologists. *PLoS Medicine*, 15(11):e1002686, 2018.
- Colorado J Reed, Xiangyu Yue, Ani Nrusimha, Sayna Ebrahimi, Vivek Vijaykumar, Richard Mao, Bo Li, Shanghang Zhang, Devin Guillory, Sean Metzger, et al. Self-Supervised Pretraining Improves Self-Supervised Pretraining. In *IEEE/CVF Winter Conference on Applications of Computer Vision (WACV)*, pages 2584–2594, 2022.
- Andrew B Sellaergren, Christina Chen, Zaid Nabulsi, Yuanzhen Li, Aaron Maschinot, Aaron Sarna, Jenny Huang, Charles Lau, Sreenivasa Raju Kalidindi, Mozziyar Etemadi, et al. Simplified Transfer Learn-

- ing for Chest Radiography Models Using Less Data. *Radiology*, 305(2):212482, 2022.
- Rebecca Smith-Bindman, Diana L Miglioretti, Eric Johnson, Choonsik Lee, Heather Spencer Feigelson, Michael Flynn, Robert T Greenlee, Randell L Kruger, Mark C Hornbrook, Douglas Roblin, et al. Use of Diagnostic Imaging Studies and Associated Radiation Exposure for Patients Enrolled in Large Integrated Health Care Systems, 1996-2010. *Jama*, 307(22):2400-2409, 2012.
- Hari Sowrirajan, Jingbo Yang, Andrew Y Ng, and Pranav Rajpurkar. Moco Pretraining improves Representation and Transferability of Chest X-Ray Models. In *Medical Imaging with Deep Learning*, pages 728-744. PMLR, 2021.
- RM Summers. NIH Chest X-Ray Dataset of 14 Common Thorax Disease Categories, 2019.
- Yu-Xing Tang, You-Bao Tang, Yifan Peng, Ke Yan, Mohammadhadi Bagheri, Bernadette A Redd, Catherine J Brandon, Zhiyong Lu, Mei Han, Jing Xiao, et al. Automated Abnormality Classification of Chest Radiographs using Deep Convolutional Neural Networks. *NPJ Digital Medicine*, 3(1):1-8, 2020.
- Yen Nhi Truong Vu, Richard Wang, Niranjan Balachandar, Can Liu, Andrew Y Ng, and Pranav Rajpurkar. Medaug: Contrastive Learning Leveraging Patient Metadata Improves Representations for Chest X-Ray Interpretation. In *Machine Learning for Healthcare Conference*, pages 755-769. PMLR, 2021.
- Xiaosong Wang, Yifan Peng, Le Lu, Zhiyong Lu, Mohammadhadi Bagheri, and Ronald M Summers. Chest X-Ray8: Hospital-scale Chest X-Ray database and benchmarks on Weakly-Supervised Classification and Localization of Common Thorax Diseases. In *IEEE/CVF Conference on Computer Vision and Pattern Recognition (CVPR)*, pages 2097-2106, 2017.
- Yuhao Zhang, Hang Jiang, Yasuhide Miura, Christopher D Manning, and Curtis P Langlotz. Contrastive Learning of Medical Visual Representations from Paired Images and Text. *arXiv preprint arXiv:2010.00747*, 2020.

Table 3: Final labels in each dataset. Underlined labels are used in the experiments with 5 labels.

| Dataset | Labels |
|-------------------------|--|
| NIH-CXR (11 labels) | <u>Consolidation</u> , Emphysema, <u>Edema</u> , <u>Atelectasis</u> , Fibrosis, Pneumothorax, Nodule/Mass, <u>Cardiomegaly</u> , <u>Effusion</u> , Hernia, Pleural Thickening |
| CheXpert (12 labels) | <u>Consolidation</u> , <u>Effusion</u> , <u>Edema</u> , Pneumothorax, Nodule/Mass, Fracture, Enlarged Cardiomeastinum, Lung Opacity, Pleural Other, <u>Cardiomegaly</u> , <u>Atelectasis</u> , Support Devices |

Appendix A. Dataset Details

Pathologically similar dataset labels were merged after consulting radiologists. This makes the dataset and our model more suitable for clinical deployment.

NIH-CXR originally contained 14 labels. We’ve merged two sets of labels - 1) Infiltration, Consolidation and Pneumonia into Consolidation, and 2) Nodule and Mass into Nodule/Mass. For CheXpert, we 1) combined Consolidation and Pneumonia, 2) renamed Lung Lesion to Nodule/Mass to maintain consistency across datasets. The no finding label was removed, as absence of all labels in the multi-label setup automatically indicates the same. The final list of labels in each dataset is shown in (*cf.* Table 3)

Appendix B. Supplementary Results

Comparison of 5 vs. all labels. We see a trend similar to SimCLR from Fig. 3 for the SwAV algorithm in Fig. 5. While the SSL PT models finetuned on NIH 5 labels still lag behind the supervised models as in the all labels setting, the SSL PT models fine-

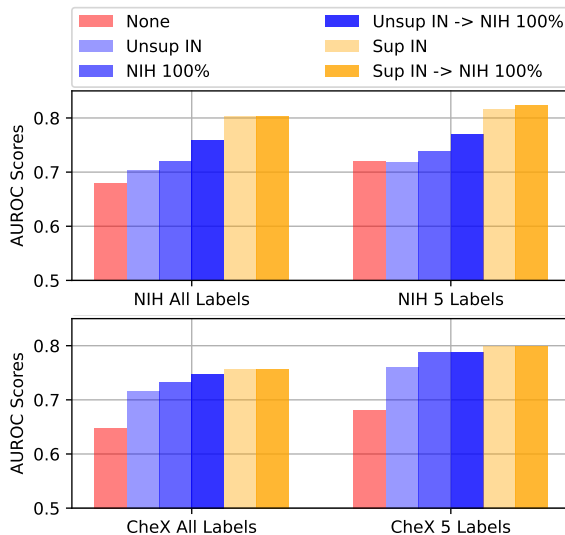


Figure 5: Comparing fine-tuning on 5 vs. all labels using the SwAV algorithm. Top: NIH, Bottom: CheXpert.

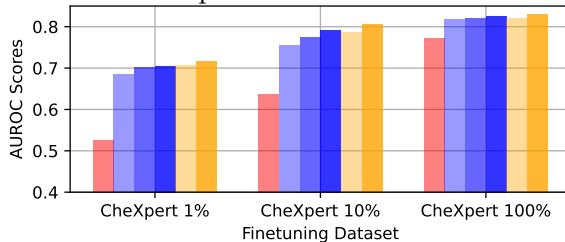


Figure 6: Zero-shot evaluation. Models are PT using the SwAV algorithm. CheXpert → NIH (5 labels).

tuned on 5 labels of CheXpert have a similar performance to those supervised PT models. This provides further evidence for the trend observed earlier.

Zero-shot evaluation. In Fig. 6, we present the results of models finetuned on CheXpert and evaluated on NIH. The SSL PT models (blue bars) are particularly strong in this setting. Chained pre-training on unlabeled ImageNet and NIH either performs at par or slightly improves the results of the supervised models. This shows the promise of pre-training on unlabeled domain data, and then fine-tuning on labeled domain data, even if it has a different labeled set.